Selective oxidation of methane to methanol using supported AuPd catalysts prepared by stabiliser-free sol-immobilisation

Christopher Williams[a], James H. Carter[a], Nicholas F. Dummer[a], Y. Kit Chow[a], David J. Morgan[a],Sara Yacob[b], Pedro Serna[b], David J. Willock[a], Randall J. Meyer[b], Stuart H. Taylor[a] and Graham J. Hutchings*[a]

[a] Cardiff Catalysis Institute, School of Chemistry, Cardiff University, CF10 3AT

[b] ExxonMobil Research and Engineering Company, Corporate Strategic Research, Annandale, NJ 08801, USA

*Corresponding email: hutch@cardiff.ac.uk

Abstract

The selective oxidation of methane to methanol, using H_2O_2, under mild reaction conditions was studied using bimetallic 1 wt. % AuPd/TiO_2 prepared by stabiliser-free sol-immobilisation. The as-prepared catalysts exhibited low, unselective oxidation activity and deleterious H_2O_2 decomposition, which was ascribed to the small mean particle size of the supported AuPd nanoparticles. Heat treatments were employed to facilitate particle size growth, yielding an improvement in the catalyst turn-over-frequency and decreasing the H_2O_2 decomposition rate. The effect of support phase was studied by preparing a range of AuPd catalysts supported on rutile TiO_2. The low surface area rutile TiO_2 yielded catalysts with effective oxygenate production, but poor H_2O_2 utilisation. The influence of the rutile-TiO_2 support was investigated further by producing catalysts with a lower metal loading to maintain a consistent metal loading per m^2 to the 1 wt.% AuPd/ P25 TiO_2 catalyst. When calcined at 800 °C the 0.13 wt.% AuPd catalyst demonstrated significantly improved turn-over frequency of 103 h^{-1}. In contrast, the turn-over frequency was found to be *ca*. 2 h^{-1} for the rutile-supported 1 wt. % AuPd catalyst calcined at 800 °C. The catalysts were probed by electron microscopy and XPS to understand the influence of particle size and oxidation state on the utilisation of H_2O_2 and oxygenate productivity. This work shows that the key to highly active catalysts involves the prevention of deleterious H_2O_2 decomposition and this can be achieved through carefully controlling the nanoparticle size, metal loading and metal oxidation state.

Keywords: methane, C-H, methanol, AuPd, particle size, partial methane oxidation

Introduction

The direct oxidation of methane to methanol is a key challenge within the scientific community.[1,2] However, the direct transformation to methanol is complicated by the intrinsic inertness of methane, which lacks a dipole moment and usually requires harsh conditions for the activation of the kinetically stable C-H bond ($\Delta H_{C\text{-}H}$ = 440 kJ mol^{-1}).[3] Current industrial methanol production is an energy-intensive and an indirect process that converts methane to synthesis gas before further conversion to methanol and other bulk chemicals.[4,5] This process demonstrates high selectivity towards the desired products producing 85 million metric tonnes of methanol per annum as well as other valuable commodities.[6]

A single step approach, applicable under low reaction temperature would therefore drastically reduce processing costs for the production of methanol. Additionally, both affordable and readily available, natural gas has the potential to be an alternative feedstock for chemicals and high value fuels, reducing the global dependence and prolonging current petroleum reserves. Natural gas is a viable prospect for an abundant feedstock with proven reserves of ca.190 trillion cubic metres.[7] Furthermore, with many natural gas reserves found in remote locations, direct conversion to methanol at the point of extraction would provide a feedstock with reduced hazards and transportation costs.

Homogeneous catalytic applications have provided important information for low temperature approaches, active site regeneration and high selectivities. However, typically these processes require harsh reaction conditions or sacrificial reagents.[8–11] Contrastingly, Hutchings and co-workers[12] have reported the use of an environmentally benign H_2O:H_2O_2 system, efficiently oxidising methane to methanol under low reaction temperatures (50 °C). The use of Fe-ZSM5 was inspired by methane mono-oxygenase, which carries out a one-step oxidation of methane to methanol under mild, aqueous conditions. The Fe- and Cu- promoted Fe-ZSM5 catalysts demonstrated considerable activity for the oxidation of methane to methanol, achieving turnover frequencies (TOFs) of > 2200 h^{-1} and methanol selectivities above 80 %.[13]

Alternatively, C-H bond activation has been extensively studied using noble metal catalysts such as AuPd.[14,15] Kesavan *et al*. [16] reported the selective oxidation of the methyl group C-H bonds in toluene over TiO_2- and carbon- supported AuPd catalysts using O_2. Demonstrating high selectivity towards benzyl benzoate the differences in catalytic activity were attributed

to different AuPd morphologies due to support-metal interactions. However, direct oxidation of methane to methanol with oxygen has proved a significant challenge. Ab Rahim *et al*.[17,18] reported on the systematic study of AuPd/TiO_2 catalysts for efficient formation of methanol from methane with H_2O_2. These catalysts were synthesized by wet impregnation from chloride precursors onto the support, typically producing a broad range of particle sizes. The catalysts were comprised of alloyed AuPd nanoparticles, with particle sizes ranging from 5-20 nm and Au-rich nanoparticles 100-200 nm in size.[19] The presence of sub-nm AuPd particles and clusters of Pd were also identified, reflecting the poor control of metal dispersion and speciation provided by wet impregnation. Even so, these AuPd/TiO_2 catalysts showed moderate activity, demonstrating the highest methanol (49%) and oxygenate selectivity (90%) of supports investigated, including carbon.[20]

Despite exhibiting lower oxygenate formation, TOF and methanol selectivity than their Fe-ZSM-5 counterparts, AuPd catalysts are an attractive class of catalyst because they could be developed to generate H_2O_2 *in situ* from H_2 and O_2. Ab Rahim *et al*., applied this approach with AuPd/TiO_2, reporting a productivity of 0.50 mol kg_{cat}^{-1} h^{-1} compared to 0.116 mol kg_{cat}^{-1} h^{-1} when similar amounts of preformed H_2O_2 (250 μmol).[18] However, an improvement in methanol selectivity (68%) and three-fold improvement in H_2O_2 reactivity were observed during *in situ* peroxide generation.

Recently Agarwal *et al*.[21] showed significant improvements in activity when unsupported AuPd nanoparticles were used. Colloidal AuPd prepared using poly(vinyl pyrrolidine) showed high oxygenate productivity with preformed H_2O_2 (29.4 mol kg_{cat}^{-1} h^{-1}). Notably, the introduction of oxygen with preformed H_2O_2 resulted in a substantial increase in oxygenate productivity to 53.6 mol kg_{cat}^{-1} h^{-1}. The use of $^{18}O_2$ demonstrated significant incorporation of the gas phase O_2 into the methanol produced (70%). Crucially however, the rate of H_2O_2 decomposition was drastically reduced by elimination of a metal-support interaction and the resulting high productivity was attributed to the controlled H_2O_2 breakdown.

Industrially, *in situ* generation of H_2O_2 is more desirable than using pre-formed H_2O_2 as the oxidant, a necessary requirement for the use of MFI-zeolite based catalysts. In order to realise this application, a solid understanding of the chemical reactivity of H_2O_2 with supported AuPd catalysts is required. In contrast to impregnation techniques, catalyst synthesis by sol-immobilisation (SI) facilitates the control of particle sizes, composition and morphology.[22,23]

This methodology has been used to tune catalyst activity and enhance product selectivity for several reactions, including benzyl alcohol oxidation and hydrogenation of furfural.[24,25] In this investigation, the role of AuPd particle size, support and oxidation state is considered for the selective oxidation of methane to methanol using added H_2O_2. The particle size distribution of AuPd is controlled using SI and carefully manipulated to evaluate the influence of nanoparticle size on the effective utilisation of H_2O_2 and the production of methanol.

Experimental

Preparation of AuPd/TiO_2 by sol-immobilisation

For 0.5 wt.% Au-0.5 wt.% Pd/TiO_2, aqueous solutions of $HAuCl_4.xH_2O$ (Aldrich 99.9% 1.667 mL, 12.25mg mL^{-1}) and $PdCl_2$ (Aldrich 0.816 mL, 6 mg mL^{-1}) were added to deionised water (800 mL) under vigorous stirring at room temperature. The resulting solution was stirred for 2 min before the addition of freshly prepared $NaBH_4$ (7.23 mL, 0.1 M) such that the molar ratio of $NaBH_4$ to metal was 5:1.[16,26] Upon the addition of $NaBH_4$, the mixture turned dark brown/black and was then vigorously stirred for 30 min before addition of the TiO_2 (P25 Degussa, 1.98 g) support. The solution was acidified to pH 1 after 1 min by drop-wise addition of sulfuric acid (>95%) and stirred for 1 h. The suspension was then filtered under vacuum and washed thoroughly with distilled water and then dried in a conventional oven for 16 h at 110 °C. Calcinations were performed under static air at various temperatures for 3 h (ramp rate of 20 °C min^{-1}), while reduction of the catalysts was carried out under flowing 5% H_2/Ar for 4 h (ramp rate = 10 °C min^{-1}).

A similar method was followed for the preparation of 0.065 wt.% Au- 0.065 wt.% Pd/rutile TiO_2 using aqueous solutions of $HAuCl_4.xH_2O$ (Aldrich 99.9% 0.1061 mL, 12.25mg mL^{-1}) and $PdCl_2$ (Aldrich 99.9% 0.2167 mL, 6 mg mL^{-1}), with pre-calcined TiO_2 (P25 Degussa, 1.9974 g) support.

In order to help differentiate between the prepared catalysts, the following nomenclature was adopted: “metal loading% AuPd/phase of TiO_2, temperature of preparation, calcination temperature”. For example, a 1 wt. % AuPd catalyst prepared at room temperature on P25 TiO_2 and calcined at 800 °C would be abbreviated as 1%AuPd/P25-RT-800. A table of the catalysts prepared and their abbreviations is presented in the Supporting Information (Table S1).

Oxidation of methane using H_2O_2

The oxidation of methane was carried out using a 50 mL Parr stainless steel autoclave reactor. The autoclave was fitted with a removable Teflon liner (35 mL volume).

Reactions were carried out using a 10 mL reaction mixture comprising an aqueous solution of H_2O_2 (10 mL, 0.5 M, 5000 µmol) and the catalyst (10 mg). Prior to use the reactor was purged with methane to remove residual air before being pressurised with methane to 30.5 bar. The autoclave was then heated to the desired reaction temperature (50 °C) using the pre-set programme. At reaction temperature (t= 0 min), the solution was vigorously stirred at 1500 RPM and both heating and stirring were maintained for the required length (typically 30 min). Following this, the stirring was stopped and the temperature was reduced to 10 °C using an ice bath to minimise the loss of volatile products. Gaseous samples were removed by extraction into a gas bag for analysis via gas chromatography. The Varian-GC was equipped with a CP-SIL5CB column (50 m, 0.33 mm internal diameter) fitted with a methaniser and analysed by a flame ionisation detector (FID). The reaction mixture was filtered to remove catalyst particulates and analysed by ^{1}H NMR, using a Bruker 500 MHz Ultra-shield NMR spectrometer. A sample NMR spectrum is presented in Figure S1. All ^{1}H NMR samples were analysed against a calibrated insert containing tetramethylsilane (TMS) in deuterated chloroform (99.9 % D). The remaining H_2O_2 was determined by titration with acidified $Ce(SO_4)_2$.

Reactions to determine the decomposition rate of H_2O_2 over catalyst samples

The decomposition of H_2O_2 was carried out in a 35 mL glass vial. A typical reaction was carried out using 10 mL reaction mixture comprising an aqueous solution of H_2O_2 (10 mL, 0.5 M, 5000 µmol) and a measured amount of solid catalyst (10 mg). At intervals, H_2O_2 concentration was determined by titration of 0.1 mL sample of reaction solution against an acidified $Ce(SO_4)_2$ solution of known concentration using one drop of ferroin indicator (0.025 M). The reactions were carried out at room temperature, with stirring maintained at 1000 RPM.

Catalyst Characterisation

Powder X-ray Diffraction (XRD) patterns were collected using a PANalytical X'PertPRO X-ray diffractometer, with Cu K_α radiation source (λ = 0.154 nm) and a Ni filter at ambient conditions. Samples were recorded between 15-80 ° at 40 kV and 40 mA with step sizes of 0.0167°.Transmission electron microscopy (TEM) was performed on a JEOL JEM-2100

operating at 200 kV. Samples were prepared by dispersion in ethanol by sonication and deposited onto 300 mesh copper grids coated with holey carbon film. X-ray photoelectron spectroscopy (XPS) was performed using a Kratos Axis Ultra DLD spectrometer, using monochromatic Al K_α X-ray source operating at 120 W. Data was collected with pass energies of 160 eV for survey spectra, and 40 eV for higher resolution scans. The system was operated in the Hybrid mode, using a combination of magnetic immersion and electrostatic lenses and acquired over an area approximately 300 $\times$ 700 μm^2. A magnetically confined charge compensation system was used to minimize charging of the sample surface, and all spectra were taken with a 90 ° take of angle. A base pressure of *ca*. 1×10^{-9} Torr was maintained during collection of the spectra. Each spectrum was calibrated against adventitious carbon, using the C 1s region, to 284.8 eV and CasaXPS was used for peak fitting, with integrated areas corrected for elemental sensitivity using modified Wagner factors as supplied by Kratos. Experimental binding energies are reported with confidence of ±0.2 eV. To assess any reduction of Pd(II) species during analysis, Pd(3d)/Au(4d) spectra were acquired both at the start and again at the end of analysis, with negligible reduction of Pd(II) noted during the total analysis period.

Surface area measurements were performed at -196 °C on a Quantachrome Quadrasorb SI instrument after each sample was evacuated for 1 h at 120 °C. Surface areas were calculated using Brunauer–Emmet–Teller (BET) theory over the range P/P0 = 0.05-0.2.

Energy dispersive X-ray analysis (EDX) was performed on a Tescan Maia3 field emission gun scanning electron microscope (FEG-SEM) fitted with an Oxford Instruments XMAXN 80 Images were acquired using the secondary electron and backscattered electron detectors. Samples were dispersed as a powder onto adhesive carbon Leit discs mounted onto aluminium stubs.

Results and Discussion

The effect of the nanoparticle size

To evaluate the effect of supported metal particle size, a series of 1 wt. % AuPd/TiO_2 (P25) catalysts were prepared using stabiliser-free sol-immobilisation. This technique can produce supported catalysts with a narrow nanoparticle size distribution which can then be manipulated with post-synthesis heat treatments.[27] Furthermore, the deposition temperature during catalyst synthesis was previously reported to affect the size of the

nanoparticles. Rogers *et al*.[28] previously reported an increase in particle size for poly(vinyl alcohol) stabilised Au nanoparticles after increasing the temperature during colloidal deposition from 25 to 70 °C. The mean particle size of resulting Au nanoparticles increased from 2.3 nm to 3.3 nm respectively.[28] Therefore, both room temperature (RT) and 70 °C were investigated so that the effect of small changes to the nanoparticle size on the resultant methane oxidation activity could be established. The mean particle size of 1%AuPd/P25-RT-dried and 1%AuPd/P25-70-dried catalysts are reported in Table 1 (Entries 3 and 7). These were calculated from representative TEM images (see supporting information Fig. S2a and Fig. S3a) from approximately 250 particles. Increasing the catalyst preparation temperature from RT to 70 °C increased the mean particle size from 4.0 nm to 5.2 nm, consistent with the previously reported size increase by Rogers *et al*.[28] The dried-only catalysts possess a particle size distribution of 2-10 nm, as shown in Figure S2a and S3a. This profile is also consistent with previously published reports where catalysts were prepared using stabiliser-free methods for sol-immobilisation.[29]

Initially, control reactions with no catalyst or just the support, TiO_2, were carried out (Table 1, Entries 1 and 2), where no oxygenates were observed. The small quantity of CO_2 detected was considered to be adventitious. The dried-only catalysts were then screened for methane oxidation and the catalytic activity data is presented in Table 1 (Entries 3 and 7). Despite the almost complete decomposition of H_2O_2 over both catalysts, no selective oxidation products were detected. We consider that the small particle size of the AuPd alloy could facilitate a rapid decomposition of the H_2O_2 to H_2O, which would prevent the possibility of methane reacting with active hydroperoxyl- or hydroxyl- radicals.[30,31] Previously, it was shown that such materials exhibit high rates of H_2O_2 productivity in the direct synthesis of H_2O_2, as well as high H_2O_2 decomposition rates (> 100 μmol min^{-1}).[31]

Larger modifications to the mean particle size were achieved through post-synthesis heat treatments at 400, 600 or 800 °C. The catalysts calcined at 400 °C (Table 1, Entries 4 and 8) did not produce oxygenates, despite an increase in the metal nanoparticle size to 6.5 nm and 7.5 nm respectively. As with the dried-only catalysts, there was no H_2O_2 remaining after the reaction. The complete decomposition of H_2O_2 by the dried-only catalysts and catalysts calcined at 400 °C is typical of materials with small particle sizes[31] and explains the low productivities observed for methane oxidation (0.054 mol kg_{cat}^{-1} h^{-1}).

Table 1: The effect of post-synthesis heat treatment on the catalytic activity of 1wt.% AuPd/TiO_2 (P25) for the oxidation of methane.[a] (Entries 3-6; room temperature, 7-10; 70°C)

Entry	Heat Treatment	Products [µmol]				Oxygenate selectivity [d] [%]	Total Productivity[e] [mol $kg_{(cat)}^{-1}$ h^{-1}]	TOF[f] [h^{-1}]	H_2O_2 Remaining[g] [%]	Mean Particle Size[h] [nm]	H_2O_2 Decomposition Rate[g][i] [µmol min^{-1}]
		Methanol[b]	Formic Acid[b]	Methyl hydroperoxide [b]	CO_2 [c]						
1	Blank	0	0	0	0.24	0	0	0	97.6	n/a	n/a
2	TiO_2	0	0	0	0.20	0	0.039	0	97.4	n/a	n/a
3	RT, Dried	0	0	0	0.27	0	0.054	0.78	0.3	4.0 ± 1.4	557
4	RT, 400 °C	0	0	0	0.27	0	0.054	0.77	0.3	6.5 ± 2.1	199
5	RT, 600 °C	0.03	0	0.13	0.16	46.6	0.063	0.91	1.7	8.3 ± 2.0	105
6	RT, 800 °C	0.23	0	0.50	0.17	80.8	0.172	2.47	42.1	19.0 ± 5.1	99
7	70 °C, Dried	0	0	0	0.16	0	0.032	0.50	0.3	5.2 ± 1.4	278
8	70 °C, 400 °C	0	0	0	0.14	0	0.018	0.28	0.5	7.5 ± 2.0	251
9	70 °C, 600 °C	0	0	0.12	0.16	42.5	0.057	0.89	13.3	11.1 ± 2.4	145
10	70 °C, 800 °C	0.29	0	1.12	0.16	90.0	0.312	4.87	56.1	19.7 ± 6.2	31

[a]Standard reaction conditions: time: 30 min, temperature: 50 °C, P_{CH4}: 30.5 bar, stirring rate: 1500 rpm, all catalysts (1 wt. % total): 7.24×10^{-7} mol of metals equal to 10 mg for solid catalysts, volume: 10 mL of H_2O.[H_2O_2]: 0.5 M. Catalysts were prepared by SI at room temperature (entries 3-6) or at 70 °C (entries 7-10). Catalyst is dried at 110 °C, 10 °C min^{-1}, 16 h, static air. Calcined at various temperatures (20 °C min^{-1}, 3 h, static air). [b] Analysed by ^{1}H NMR spectroscopy with 1 % TMS in $CDCl_3$ internal standard. [c] Analysed by gas chromatography using an FID methaniser . Values obtained using CO_2 calibration curve. [d] Oxygenate selectivity calculated as (moles oxygenates/total moles of products) x 100. [e] Total productivity calculated as (moles(products) /weight(catalyst))/time). [f] TOF: Turn-over frequency, calculated as (moles(products) / total moles(metal)) / time (h). [g]Remaining H_2O_2 assayed by Ce^{4+} (aq.) titration. Calculated as (moles(initial)/moles(final) x100. [h] Determined by transmission electron microscopy. [i] H_2O_2 decomposition reaction conditions: time: 30mins, temperature: 24 °C, atmospheric pressure, stirring rate: 1000rpm, all catalysts (1 wt. % total): 7.24×10^{-7} mol of metals equal to 10 mg for solid catalysts, volume: 10 mL of H_2O.[H_2O_2]: 0.5 M. Maximum experimental error; Methanol: 10%, Methyl Hydroperoxide: 16%, CO_2: 22%, H_2O_2: 9%.

In order to better establish the relative rate of H_2O_2 decomposition, a series of control experiments at room temperature were performed. The catalysts were stirred in a dilute H_2O_2 solution and the decomposition rate was determined through analysis of the solution as a function of time. The decomposition rates expressed as μmol min^{-1} are reported in Table 1 and the time-on-line data is shown in supporting information Figure S4 and S5. The rate of H_2O_2 decomposition over 1%AuPd/P25-RT-dried was found to be 557 μmol min^{-1} and 278 μmol min^{-1} for 1%AuPd/P25-70-dried. Less than 10 % of the H_2O_2 was remaining after 30 min and indicates that the small AuPd particles are capable of rapidly decomposing H_2O_2.

Following heat treatment at 600 °C (Table 1, Entries 5 and 9) the particle sizes of the catalysts increased to *ca*. 10 nm, where the onset of catalytic activity was observed, albeit with low productivity and relatively high H_2O_2 decomposition rates. The rate of H_2O_2 decomposition decreased to *ca*. 100 μmol min^{-1} over these catalysts, although just 1.7 % of H_2O_2 remained after the oxidation reaction. The rate of H_2O_2 decomposition over catalysts with metal nanoparticles less than 8 nm in diameter is unfavourably high and does not facilitate the production of methanol.

Heat treatment at 800 °C (Table 1, Entries 6 and 10) resulted in a significant growth of the mean nanoparticle size to *ca*. 19 nm in 1%AuPd/P25-RT-800 and 1%AuPd/P25-70-800 catalysts, which was matched by a large improvement in catalyst productivity (0.172 mol and 0.312 kg_{cat}^{-1} h^{-1} respectively), as well as oxygenate selectivity and remaining H_2O_2. The H_2O_2 decomposition rates of the 1%AuPd/P25-RT-800 and 1%AuPd/P25-70-800 were found to be *ca*. 100 and 30 μmol min^{-1} respectively, which emphasises that larger nanoparticles are required to ensure a sufficient concentration of reactive oxidising radicals, which facilitates the activation of methane.

Particle size distributions for both 1%AuPd/P25-RT-800 and 1%AuPd/P25-70-800 (Fig. S1d and S2d) demonstrate quite similar profiles and average particle sizes: 19.0 ± 5.1 and 19.7 ± 6.2 nm, respectively. Upon closer inspection, however, the presence of nanoparticles below 9 nm in the 1%AuPd/P25-RT-800 catalyst were observed, in contrast to 1%AuPd/P25-70-800. The presence of these sub-10 nm particles could be a contributing factor in the lower activity observed with 1%AuPd/P25-RT-800, as these particles demonstrably catalyse the deleterious decomposition of H_2O_2, however the number of sub-10 nm metal nanoparticles in 1%AuPd/P25-RT-800 represents a small proportion of the total population of supported

nanoparticles. Another possible explanation concerns the standard deviation of the average particle size measurements, which suggests that the actual differences in the supported nanoparticle sizes are greater than suggested by the average value. There are, however, clear trends associated with the average particle sizes, the rates of H_2O_2 decomposition and the quantity of reaction products. These relationships are illustrated in Figure 1 a), b) and c).

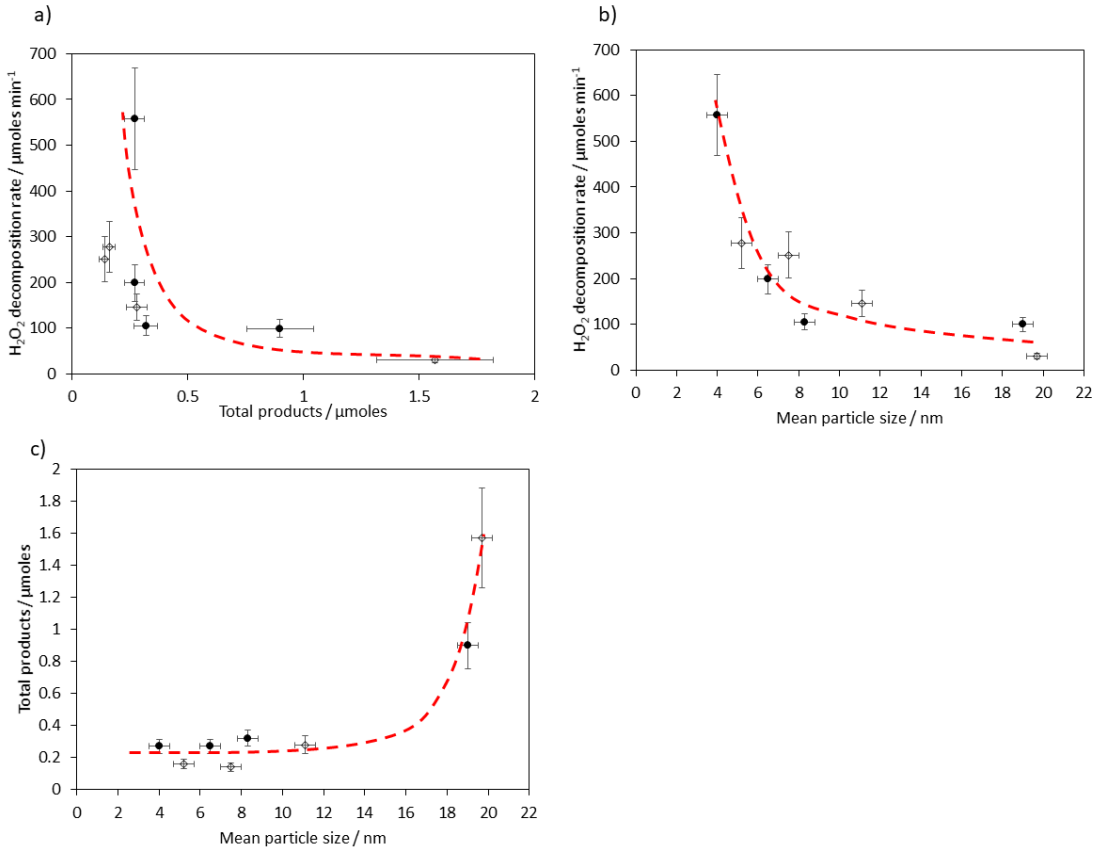

Fig. 1. The structure-activity relationship of 1 wt. % AuPd/ TiO_2 (P25) for methane oxidation: a) Lower H_2O_2 decomposition rates are consistent with the larger quantities of products after the 0.5 h reaction; b) Lower H_2O_2 decomposition rates lead to a higher productivity after the 30 min reaction; c) Larger mean particle sizes result in higher productivities. ● = RT and ◊ = 70 °C.

The oxidation state of Pd has previously been demonstrated to affect the rate of H_2O_2 decomposition[32,33]. XPS was therefore used to investigate a potential link between H_2O_2 decomposition rates (and therefore oxygenate production) and the oxidation state of Pd in the samples. The corresponding Au 4d and Pd 3d spectra are illustrated in Figure S7 and S8, with elemental analysis provided in Table S2. It is evident that the preparation method, involving $NaBH_4$ as the reducing agent, leads to the formation of the reduced metal species only. Expectedly, calcination of the catalysts resulted in the formation of oxidised species, with only Pd^{2+} present after calcination at 400 °C (Fig. S7 and S8) (Table S2, Entries 2-4 and 6-

8). Overall, the XPS analysis of Pd 3d region of the RT and 70 °C prepared samples was similar and the oxidation state of the Pd was not affected by the temperature of the preparation method. In order to confirm the metal loadings and Au:Pd ratio, elemental analysis was carried out on the dried samples using MP-AES after digestion of the catalysts using *aqua regia*. Due to inefficient digestion of TiO_2 support when using *aqua regia*, complementary SEM-EDX analysis was also carried out. The measured metal loadings are presented in Table S2 and are very close to that of the nominal values, although the 1%AuPd-P25-70-800 had a lower loading (0.89 wt.%) than 1%AuPd-P25-RT-800 (0.97 wt.%). Additionally, these SEM-EDX measurements were also consistent with the MP-AES data. The lower loading of metal in 1%AuPd-P25-70-800 could actually be beneficial as there are fewer sites to decompose H_2O_2 in the system. It was previously reported that increasing the mass of 5 wt. % AuPd/TiO_2 catalysts could lower the production of methanol.[18] The importance of the concentration of metal is discussed below. TOFs were calculated according to the total metal loading determined using MP-AES (Table 1). The most active catalyst, 1%AuPd-P25-70-800, exhibited a TOF of 4.87 h^{-1}, comparable to those previously reported.[20]

The effect of the support phase

The increase in oxygenate productivity noted when the 1 wt. % AuPd/TiO_2 (P25) catalysts were calcined at 800 °C was ascribed to the increase in mean AuPd particle size, which prevented the deleterious decomposition of H_2O_2. However, the P25 TiO_2 support also underwent a phase transition to rutile, as evidenced by the characteristic XRD reflections (Fig. S6). Therefore, an analogous series of catalysts were prepared on rutile TiO_2. Nitrogen adsorption measurements indicated that the BET surface area decreased from 45 $m^2\ g^{-1}$ for the P25 material to 6 $m^2\ g^{-1}$ for the rutile material. Catalysts were prepared with 1 wt.% AuPd at both room temperature and at 70 °C for consistency with the previous samples and were tested for the selective oxidation of methane with H_2O_2 (Table 2) after the same heat treatments. The XRD patterns of the supported rutile catalysts are shown in Fig. S9, and indicate that no major phase changes occur to the catalyst support. Consistent with the results in Table 1, selective methane oxidation over 1 wt.% AuPd/rutile was not observed for the dried-only catalysts prepared at RT or 70 °C (Table 2, Entries 2 and 6). These catalysts exhibited high H_2O_2 decomposition activity (Fig. S12 and S13), which we consider is due to the

particle size and presence ofmetallic Pd in the AuPd nanoparticles. Analysis of the rutile-supported catalysts by TEM revealed an interesting phenomenon that occurs during preparation (Fig. S10 and S11). Deposition of stabiliser-free AuPd sols onto the rutile TiO_2 support resulted in particle agglomerates on the dried-only catalyst, rather than discrete nanoparticles. Heat treatment of these parent catalysts subsequently resulted in the preferential formation of distinct, hemi-spherical nanoparticles, which increase in size with increasing heat treatment temperatures (Fig. S10 and S11). Interestingly, the AuPd/rutile catalysts calcined at 400 °C exhibited selective catalytic activity towards oxygenates (Table 2, Entries 3-5 and 7-9), in contrast to the analogous catalysts supported on P25. After calcination at 800 °C, the mean particle size increased to 19 - 23 nm, consistent with the catalysts supported on the untreated TiO_2 support.

Table 2: The effect of support pre-calcination for 1wt.% AuPd/rutile TiO_2 prepared at room temperature (Entries 2-5) and at 70 °C (Entries 6-9)[a]

Entry	Heat Treatment	Products [µmol]				Oxygenate selectivity [d] [%]	Total Productivity [e] [mol $kg_{(cat)}^{-1}$ h^{-1}]	TOF[f] [h^{-1}]	H_2O_2 Remaining[g] [%]	Mean Particle Size[h] [nm]	H_2O_2 Decomposition Rate [µmol min^{-1}]
		Methanol[b]	Formic Acid[b]	Methyl hydroperoxide[b]	CO_2[c]						
1	rutile	0	0	0	0.33	0	0.040	0	97.5	n/a	n/a
2	RT, Dried	0	0	0	0.26	0	0.052	0.73	0.2	n/a	830
3	RT, 400 °C	0.26	0	0	0.29	47.9	0.109	1.51	2.2	8.7 ± 3.9	251
4	RT, 600 °C	0.22	0	0.36	0.31	65.4	0.176	2.45	4.5	10.4 ± 2.3	147
5	RT, 800 °C	0.45	0	0.21	0.18	83.4	0.163	2.27	2.1	19.6 ± 5.9	317
6	70 °C, Dried	0	0	0	0.27	0	0.053	0.83	0.2	n/a	530
7	70 °C, 400 °C	0.36	0	0.56	0.15	86.2	0.214	3.35	1.4	8.0 ± 2.4	236
8	70 °C, 600 °C	0.30	0	0.73	0.15	87.1	0.161	2.53	23.8	10.8 ± 2.9	243
9	70 °C, 800 °C	0.38	0	0.73	0.16	86.5	0.243	3.80	7.8	22.6 ± 10.7	158

[a]Standard reaction conditions: time: 30 min, temperature: 50 °C, P_{CH4}: 30.5 bar, stirring rate: 1500 rpm, all catalysts (1 wt. % total): $7.24x10^{-7}$ mol of metals equal to 10 mg for solid catalysts, volume: 10 mL of H_2O.[H_2O_2]: 0.5 M. TiO_2 support pretreated by calcination at 800 °C prior to use in catalyst preparation (denoted rutile). Catalysts were prepared by SI at room temperature (entries 2-5) or at 70 °C (entries 6-9). Catalyst is dried at 110 °C, 10 °C min^{-1}, 16 h, static air. Calcined at various temperatures (20 °C min^{-1}, 3 h, static air). [b] Analysed by ^{1}H NMR spectroscopy with 1 % TMS in $CDCl_3$ internal standard. [c] Analysed by gas chromatography using an FID methaniser. Values obtained using CO_2 calibration curve. [d] Oxygenate selectivity calculated as (moles oxygenates/total moles of products) x 100. [e] Total productivity calculated as (moles(products) /weight(catalyst))/time). [f] TOF: Turn-over frequency, calculated as (moles(products) / total moles(metal)) / time (h). [g]Remaining H_2O_2 assayed by Ce^{4+}(aq.) titration. Calculated as (moles(initial)/moles(final) x100. [h] Determined by transmission electron microscopy.[i] H_2O_2 decomposition reaction conditions: time: 30mins, temperature: 24 °C, atmospheric pressure, stirring rate: 1000 rpm, all catalysts (1 wt. % total): $7.24x10^{-7}$ mol of metals equal to 10 mg for solid catalysts, volume: 10 mL of H_2O.[H_2O_2]: 0.5 M. Maximum experimental error; Methanol: 11%, Methyl Hydroperoxide: 16%, CO_2: 22%, H_2O_2: 10%.

However, the concentration of H_2O_2 remaining is inconsistent with our earlier observations where the presence of larger AuPd particles resulted in high percentage of H_2O_2 remaining (Table 1). For example, the 1%AuPd-rutile-RT-800 catalyst had a mean particle size of *ca*. 20 nm and exhibited high oxygenate selectivity, but with < 10 % H_2O_2 remaining (Table 2). The rate of H_2O_2 decomposition of the calcined catalysts was investigated and found to be between 150 and 317 μmol min^{-1} for the catalysts prepared at room temperature and 70 °C, respectively (Table 2, entries 3-5 and 7-9, and Fig. S12 and S13). The surface composition, as determined by XPS, indicates that between 40-60% of the Pd is present as Pd^0 (Fig. S14 and S15, and Table S3), whereas the P25 supported catalysts were composed entirely of Pd^{2+}. Previous studies on the direct synthesis of hydrogen peroxide have demonstrated Pd^0 leads to higher rates of H_2O_2 decomposition compared to Pd^{2+}.[34] The expected effect on catalytic activity would be detrimental and result in inefficient utilisation of H_2O_2. To observe the effect of Pd oxidation state on the catalytic activity, two samples of 1%AuPd/P25 were heated under a reducing environment (5% H_2/Ar) at 400 or 800 °C and screened for methane oxidation. The results of these tests are presented in Table S4 and show almost complete consumption of H_2O_2, and almost no catalytic activity. These data confirm that Pd^0 promotes H_2O_2 decomposition at the expense of methane oxidation activity.

The large mean particle sizes and the presence of Pd^0 observed with the heat-treated catalysts supported on rutile TiO_2 suggest that this combination can facilitate both the selective oxidation of methane whilst exhibiting an increased rate of H_2O_2 decomposition. This combination however does not facilitate efficient utilisation of H_2O_2. This is evident in Fig. 2, which depicts comparable relationships to those plotted in Fig. 1. The mean particle size of the rutile-supported catalysts does not correlate well with H_2O_2 decomposition or total products, as the Pd oxidation state is evidently an important parameter in determining these rates. Analogous elemental analysis using MP-AES and EDX was carried out on the rutile supported catalysts to confirm the expected metal loadings (Table S3). In each case, the metal loadings are close to the nominal loadings, although the catalysts prepared at 70 °C had a marginally lower total metal loading (0.91 wt. %), consistent with the P25-supported catalysts, suggesting that the interaction of the nanoparticles and the support is less favourable at elevated temperatures. Additionally, the increased performance of the 1%AuPd-rutile-70-800 compared with 1%AuPd-rutile-RT-800 could, in part, be due to the lower concentration of metal. Not only does this increase the TOF, but the lower metal

loading is also consistent with higher productivity, which as suggested above, could contribute to suppressing the deleterious decomposition of H_2O_2.

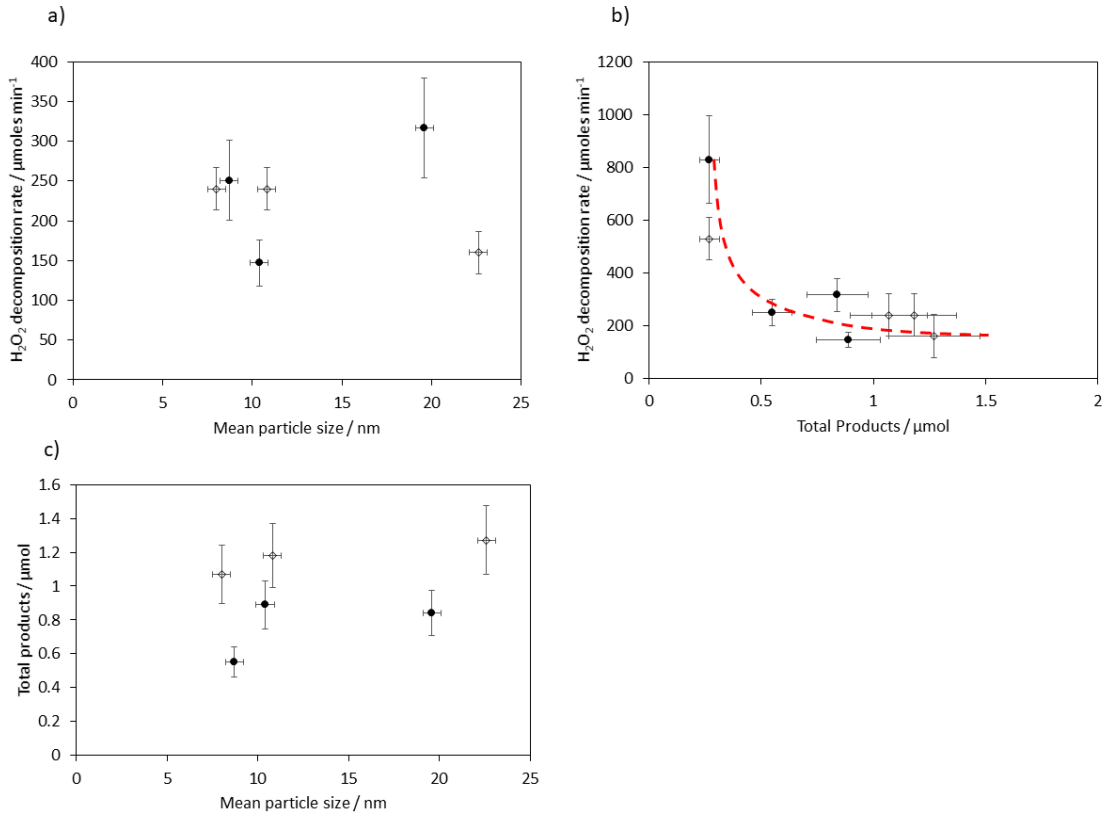

Fig. 2. The structure-activity relationship of 1 wt. % AuPd/ TiO_2 (rutile) for methane oxidation: a) In contrast to the P25-supported catalyst, there is not a clear correlation between the H_2O_2 decomposition rate and the mean particle size; b) The H_2O_2 decomposition rate correlates well with the total products after the 0.5 h reaction: c) The correlation between mean particle size and total products for catalysts prepared on rutile is poor, indicating that there are other factors affecting the activity. ● = RT and ◊ = 70 °C.

The effect of surface area: metal loading ratio

The reduction in the surface area caused by the high temperature phase-change at 800 °C resulted in an increase in the supported metal to surface area ratio. Therefore, the metal loading on rutile TiO_2 was reduced from 0.167 %AuPd m^{-2} to the equivalent loading of 0.022 wt. % AuPd m^{-2}, which is consistent with the metal:surface area of the 1 wt. % AuPd/P25 TiO_2. In this case, a nominal 0.13 wt. % loading of AuPd was used to prepare catalysts at room temperature on rutile TiO_2. As expected, the mean AuPd particle sizes of the 0.13 wt. % rutile TiO_2 catalysts were comparable to the 1 wt. % AuPd/P25 TiO_2 catalysts (Table 1) although interestingly, the dried catalyst featured nanoparticles that had formed agglomerates as was observed in the 1 wt.% AuPd/rutile TiO_2 catalysts. Fig. S16 illustrates the observed

agglomeration, and similarly shows the formation of hemispherical nanoparticles after heat treatment at 400 °C. The 0.13 wt. % AuPd catalysts were active after calcination at 400 °C (Table 3), where the mean particle size was 6.5 nm. Furthermore, the rate of H_2O_2 decomposition for all heat-treated catalysts was low and in general, > 90 % remained after the 30 min reaction. The most likely explanation for this difference in catalytic activity is that the 0.13 wt. % AuPd catalyst had significantly less metal present per moles of reactant and, therefore, the rate of H_2O_2 decomposition was lower. The total productivity was calculated to be 0.68 mol kg_{cat}^{-1} h^{-1}, which corresponded to a turnover frequency of 103 h^{-1}, significantly higher than the 1 wt. % AuPd catalysts (2-4 h^{-1}) and any previously reported supported-AuPd bimetallic catalyst for this reaction.[18,20] As above, the TOFs were calculated according to the MP-AES measurements, which indicated the total metal loading to be 0.11 wt.%, although at these very low loadings the limit of reliable quantification is approached.

Table 3: The effect of reduced metal loading on pre-calcined support for the oxidation of methane (0.13 wt.% AuPd/rutile TiO_2) [a]

Entry	Heat Treatment	Products [µmol]				Oxygenate selectivity[d] [%]	Total Productivity[e] [mol $kg_{(cat)}^{-1}$ h^{-1}]	TOF [f] [h^{-1}]	H_2O_2 Remaining[g] [%]	Mean Particle Size[h] [nm]	H_2O_2 Decomposition Rate[g][i] [µmol min^{-1}]
		Methanol[b]	Formic Acid[b]	Methyl hydroperoxide[b]	CO_2[c]						
1	Dried	0	0	0	0.23	0	0.046	7.00	8.9	n/a	215
2	400 °C	0.06	0.00	0.41	0.25	64.8	0.152	23.0	55.1	6.5 ± 1.7	10.7
3	600 °C	0.13	0.00	0.86	0.33	75.0	0.234	35.5	75.5	9.3 ± 3.2	25.9
4	800 °C	0.32	0.19	2.65	0.27	90.7	0.677	103	64.3	19.1 ± 4.5	21.4

[a]Standard reaction conditions: time: 30 min, temperature: 50 °C, PCH4: 30.5 bar, stirring rate: 1500 rpm, all catalysts (1 wt. % total): 9.41×10^{-8} mol of metals equal to 10 mg for solid catalysts, volume: 10 mL of H_2O.[H_2O_2]: 0.5 M. TiO_2 support pretreated by calcination at 800 °C prior to use for catalyst preparation (denoted rutile TiO_2). Catalyst prepared by SI at 70 °C. Catalyst is dried at 110 °C, 10 °C min^{-1}, 16 h, static air. Calcined at various temperatures (20 °C min^{-1}, 3 h, static air). [b] Analysed by ^{1}H NMR NMR spectroscopy with 1% TMS in $CDCl_2$ internal standard. [c] Analysed by gas chromatography using a FID methaniser. Values obtained using CO_2 calibration curve. [d] Oxygenate selectivity calculated as (moles oxygenates/total moles of products) x 100. [e] Total productivity calculated as (moles(oxygenates) /weight(catalyst))/time). [f] TOF: Turn-over frequency, calculated as (moles(products) / total moles(metal)) / time (h). [g]Remaining H_2O_2 assayed by Ce^{4+}(aq.) titration. Calculated as (moles(initial)/moles(final) x100. [g] Determined by transmission electron microscopy. [h] [i] H_2O_2 decomposition reaction conditions: time: 30mins, temperature: 24 °C, atmospheric pressure, stirring rate: 1000rpm, all catalysts (1wt. % total): 7.24×10^{-7} mol of metals equal to 10 mg for solid catalysts, volume: 10 mL of H_2O.[H_2O_2]: 0.5 M. Maximum experimental error; Methanol: 13%, Formic Acid 2%: , Methyl hydroperoxide: 15%, CO_2: 20%, H_2O_2: 9%.

The rate of H_2O_2 decomposition at room temperature was much lower after calcination (Table 3, Fig. S17), as expected based on the methane oxidation reactions and the lower concentration of metal in the reaction. Over each catalyst, the rates were measured at < 26 μmol min^{-1} despite the presence of *ca*. 50 % Pd^0, as shown from XPS analysis (Table S5 and Fig. S18). This is consistent with the 1 wt.% AuPd/rutile TiO_2 catalysts that also featured high concentrations of Pd^0 after calcination, suggesting that rutile stabilises Pd^0 (or inhibits Pd oxidation). In addition, the XRD patterns of the 0.13 wt.% AuPd catalysts exhibited the same reflections as those in the 1 wt% AuPd/rutle catalysts (Fig. S19). The reduction in metal loading also decreased the concentration of H_2O_2 decomposing metal, which facilitates a slower turnover of H_2O_2 and a higher methane oxidation activity. This observation supports the work of Han[35] *et al*. and Landon[36] *et al*. who demonstrated the proportional increase in H_2O_2 hydrogenation with increasing catalyst mass. The results from the present work indicates that the concentration of metal is an important parameter in determining methane oxidation activity in AuPd catalysts. This relationship is illustrated in Fig. 3, demonstrating the dependence of TOF as a function of the actual metal loading, as determined from MP-AES. Catalysts calcined at 800 °C were selected due to a comparable metal nanoparticle size of *ca*. 20 nm. Further inspection (Fig. 3, Inset) shows metal loadings closer to 1 wt. % where it is evident that a lower metal loading is conducive to an improved TOF of methanol and is likely caused by a decrease in the rate of deleterious H_2O_2 decomposition. These findings further underline the sensitivity of this reaction to the properties of the catalyst.

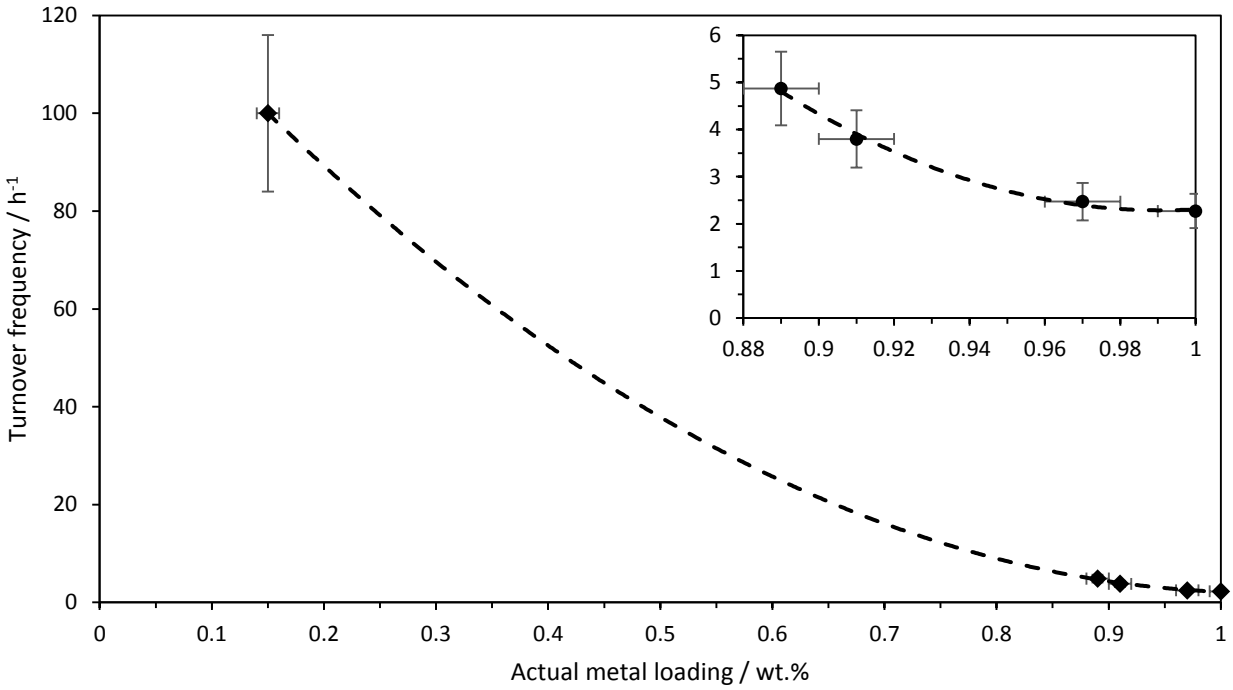

Fig. 3. The relationship between the actual metal loading determined using MP-AES and the TOF for a series of $AuPd/TiO_2$ catalysts calcined at 800 °C and with similar average particle sizes (ca. 20 nm). Inset: Close-up of the graph where the metal loading is between 0.88 - 1 wt.%.

Conclusions

The influence of nanoparticle size and Pd oxidation state on the selective methane oxidation using AuPd/TiO_2 has been systematically investigated. Using stabiliser-free sol-immobilisation, the initial particle size distribution was controlled and modification of the deposition temperature allowed small differences in the initial particle size to be induced. These dried-only catalysts were not active for methane oxidation due to their ability to rapidly decompose H_2O_2. Calcining the catalysts at 400, 600 and 800 °C resulted in significant increases in the mean particle sizes, which yielded improvements in the H_2O_2 stability. In catalysts with larger than *ca*. 10 nm metal nanoparticles, the production of oxygenates was observed. After calcination at 800 °C the P25 TiO_2 transformed from approximately 80% anatase and 20% rutile to 100% rutile. To understand the influence of the support phase, catalysts were prepared using calcined P25 TiO_2, which produced a pure rutile phase. The stabilisation of Pd^0 in these catalysts, even after high temperature calcination, resulted in rapid H_2O_2 decomposition. The metal loading was proportionally lowered to account for the lower surface area of the rutile catalyst compared to the P25 TiO_2. These 0.13 wt.% AuPd/rutile TiO_2 catalysts exhibited extremely high activity, particularly when calcined at 800 °C: The TOF of 0.13%AuPd/rutile-RT-800 was 103 h^{-1}. This is significantly higher than previously reported AuPd catalysts. We consider that the low concentration of metal in the low-loaded catalysts limited the H_2O_2 decomposition to a favourable rate. Therefore, while the supported nanoparticle size is an important parameter, it is not the only consideration that must be made in developing highly active, efficient heterogeneous catalysts for the selective oxidation of methane to methanol using supported AuPd nanoparticles. The size, oxidation state and concentration of supported nanoparticles must be controlled to maximise the efficiency and performance of the resulting catalyst.

Acknowledgements

The authors wish to thank ExxonMobil for financial support and the Cardiff University electron microscopy facility for the transmission (TEM) and scanning electron microscopy (SEM).

Associated Content

Summary of prepared catalysts, typical ^{1}H NMR spectrum of post-reaction reaction solution, TEM, H_2O_2 decomposition reaction data, XRD, XPS, MP-AES and SEM-EDX analysis of catalysts.

References

(1) da Silva, M. J. Synthesis of Methanol from Methane: Challenges and Advances on the Multi-Step (Syngas) and One-Step Routes (DMTM). *Fuel Process. Technol.* **2016**, *145*, 42–61.

(2) Horn, R.; Schlögl, R. Methane Activation by Heterogeneous Catalysis. *Catal. Letters* **2015**, *145*, 23–39.

(3) Blanksby, S. J.; Ellison, G. B. Bond Dissociation Energies of Organic Molecules. *Acc. Chem. Res.* **2003**, *36*, 255–263.

(4) Tang, P.; Zhu, Q.; Wu, Z.; Ma, D. Methane Activation: The Past and Future. *Energy Environ. Sci.* **2014**, *7*, 2580–2591.

(5) Wilhelm, D. J.; Simbeck, D. R.; Karp, A. D.; Dickenson, R. L. Syngas Production for Gas-to-Liquids Applications: Technologies, Issues and Outlook. *Fuel Process. Technol.* **2001**, *71*, 139–148.

(6) Sheldon, D. Methanol Production – A Technical History. *Johnson Matthey Technol. Rev.* **2017**, *61*, 172–182.

(7) BP Statistical Review of World Energy June 2017. https://www.bp.com/content/dam/bp/en/corporate/pdf/energy-economics/statistical-review-2017/bp-statistical-review-of-world-energy-2017-full-report.pdf.

(8) N. F. Goldshle, A. A. Shteinman, A. E.; Shilov, V. V. E. No Title. *Russ. J. Phys. Chem. USSR* **1972**, *46*, 785–786.

(9) Shilov, A. E.; Shul'pin, G. B. Activation of C−H Bonds by Metal Complexes. *Chem. Rev.* **1997**, *97*, 2879–2932.

(10) Periana, R. A.; Taube, D. J.; Evitt, E. R.; Löffler, D. G.; Wentrcek, P. R.; Voss, G.; Masuda, T.; L6ffler, D. G. A Mercury-Catalyzed, High-Yield System for the Oxidation of Methane to Methanol. *Science.* **1993**, *259*, 340–343.

(11) Periana, R. A.; Taube, D. J.; Gamble, S.; Taube, H.; Satoh, T.; Fujii, H. Platinum Catalysts for the High-Yield Oxidation of Methane to a Methanol Derivative. *Science.* **1998**, *280*, 560–564.

(12) Hammond, C.; Forde, M. M.; Ab Rahim, M. H.; Thetford, A.; He, Q.; Jenkins, R. L.; Dimitratos, N.; Lopez-Sanchez, J. A.; Dummer, N. F.; Murphy, D. M.; et al. Direct Catalytic Conversion of Methane to Methanol in an Aqueous Medium by Using Copper-Promoted Fe-ZSM-5. *Angew. Chemie - Int. Ed.* **2012**, *51*, 5129–5133.

(13) Hammond, C.; Dimitratos, N.; Lopez-Sanchez, J. A.; Jenkins, R. L.; Whiting, G.; Kondrat, S. A.; Ab Rahim, M. H.; Forde, M. M.; Thetford, A.; Hagen, H.; et al. Aqueous-Phase Methane Oxidation over Fe-MFI Zeolites; Promotion through Isomorphous Framework Substitution. *ACS Catal.* **2013**, *3*, 1835–1844.

(14) Enache, D. I.; Barker, D.; Edwards, J. K.; Taylor, S. H.; Knight, D. W.; Carley, A. F.; Hutchings, G. J. Solvent-Free Oxidation of Benzyl Alcohol Using Titania-Supported Gold–palladium Catalysts: Effect of Au–Pd Ratio on Catalytic Performance. *Catal. Today* **2007**, *122*, 407–411.

(15) Dimitratos, N.; Lopez-Sanchez, J. A.; Hutchings, G. J. Selective Liquid Phase Oxidation with Supported Metal Nanoparticles. *Chem. Sci.* **2012**, *3,* 20–44.

(16) Kesavan, L.; Tiruvalam, R.; Rahim, M. H. A.; bin Saiman, M. I.; Enache, D. I.; Jenkins, R. L.; Dimitratos, N.; Lopez-Sanchez, J. A.; Taylor, S. H.; Knight, D. W.; et al. Solvent-Free Oxidation of Primary Carbon-Hydrogen Bonds in Toluene Using Au-Pd Alloy Nanoparticles. *Science.* **2011**, *331*, 195–199.

(17) Ab Rahim, M. H.; Forde, M. M.; Hammond, C.; Jenkins, R. L.; Dimitratos, N.; Lopez-Sanchez, J. A.; Carley, A. F.; Taylor, S. H.; Willock, D. J.; Hutchings, G. J. Systematic Study of the Oxidation of Methane Using Supported Gold Palladium Nanoparticles under Mild Aqueous Conditions. *Top. Catal.* **2013**, *56*, 1843–1857.

(18) Ab Rahim, M. H.; Forde, M. M.; Jenkins, R. L.; Hammond, C.; He, Q.; Dimitratos, N.; Lopez-Sanchez, J. A.; Carley, A. F.; Taylor, S. H.; Willock, D. J.; et al. Oxidation of Methane to Methanol with Hydrogen Peroxide Using Supported Gold-Palladium Alloy Nanoparticles. *Angew. Chemie - Int. Ed.* **2013**, *52,* 1280–1284.

(19) Edwards, J. K.; Solsona, B. E.; Landon, P.; Carley, A. F.; Herzing, A.; Kiely, C. J.; Hutchings, G. J. Direct Synthesis of Hydrogen Peroxide from H_2 and O_2 Using TiO_2-Supported Au-Pd Catalysts. *J. Catal.* **2005**, *236*, 69–79.

(20) Ab Rahim, M. H.; Armstrong, R. D.; Hammond, C.; Dimitratos, N.; Freakley, S. J.; Forde, M. M.; Morgan, D. J.; Lalev, G.; Jenkins, R. L.; Lopez-Sanchez, J. A.; et al. Low Temperature Selective Oxidation of Methane to Methanol Using Titania Supported Gold Palladium Copper Catalysts. *Catal. Sci. Technol.* **2016**, *6*, 3410–3418.

(21) Agarwal, N.; Freakley, S. J.; McVicker, R. U.; Althahban, S. M.; Dimitratos, N.; He, Q.; Morgan, D. J.; Jenkins, R. L.; Willock, D. J.; Taylor, S. H.; et al. Aqueous Au-Pd Colloids Catalyze Selective CH_4 Oxidation to CH_3OH with O_2 under Mild Conditions. *Science.* **2017**, *358*, 223–227.

(22) Villa, A.; Wang, D.; Veith, G. M.; Vindigni, F.; Prati, L. Sol Immobilization Technique: A Delicate Balance between Activity, Selectivity and Stability of Gold Catalysts. *Catal. Sci. Technol.* **2013**, *3*, 3036–3041.

(23) Signoretto, M.; Menegazzo, F.; Di Michele, A.; Fioriniello, E. Effects of Support and Synthetic Procedure for Sol-Immobilized Au Nanoparticles. *Catalysts* **2016**, *6*, 87.

(24) Campisi, S.; Ferri, D.; Villa, A.; Wang, W.; Wang, D.; Kröcher, O.; Prati, L. Selectivity Control in Palladium-Catalyzed Alcohol Oxidation through Selective Blocking of Active Sites. *J. Phys. Chem. C* **2016**, *120*, 14027–14033.

(25) Rogers, S. M.; Catlow, C. R. A.; Chan-Thaw, C. E.; Chutia, A.; Jian, N.; Palmer, R. E.; Perdjon, M.; Thetford, A.; Dimitratos, N.; Villa, A.; et al. Tandem Site- and Size-Controlled Pd Nanoparticles for the Directed Hydrogenation of Furfural. *ACS Catal.* **2017**, *7*, 2266–2274.

(26) He, Q.; Miedziak, P. J.; Kesavan, L.; Dimitratos, N.; Sankar, M.; Lopez-Sanchez, J. A.; Forde, M. M.; Edwards, J. K.; Knight, D. W.; Taylor, S. H.; et al. Switching-off Toluene Formation in the Solvent-Free Oxidation of Benzyl Alcohol Using Supported Trimetallic Au-Pd-Pt Nanoparticles. *Faraday Discuss.* **2013**, *162*, 365–378.

(27) Prati, L.; Villa, A. Gold Colloids: From Quasi-Homogeneous to Heterogeneous Catalytic Systems. *Acc. Chem. Res.* **2014**, *47*, 855–863.

(28) Rogers, S. M.; Catlow, C. R. A.; Chan-Thaw, C. E.; Gianolio, D.; Gibson, E. K.; Gould, A. L.; Jian, N.; Logsdail, A. J.; Palmer, R. E.; Prati, L.; et al. Tailoring Gold Nanoparticle Characteristics and the Impact on Aqueous-Phase Oxidation of Glycerol. *ACS Catal.* **2015**, *5*, 4377–4384.

(29) Abis, L.; Freakley, S. J.; Dodekatos, G.; Morgan, D. J.; Sankar, M.; Dimitratos, N.; He, Q.; Kiely, C. J.; Hutchings, G. J. Highly Active Gold and Gold–Palladium Catalysts Prepared by Colloidal Methods in the Absence of Polymer Stabilizers. *ChemCatChem* **2017**, *15*, 2914–2918.

(30) Hutchings, G. J.; Kiely, C. J. Strategies for the Synthesis of Supported Gold Palladium Nanoparticles with Controlled Morphology and Composition. *Acc. Chem. Res.* **2013**, *46*, 1759–1772.

(31) Pritchard, J.; Kesavan, L.; Piccinini, M.; He, Q.; Tiruvalam, R.; Dimitratos, N.; Lopez-Sanchez, J. A.; Carley, A. F.; Edwards, J. K.; Kiely, C. J.; et al. Direct Synthesis of Hydrogen Peroxide and Benzyl Alcohol Oxidation Using Au-Pd Catalysts Prepared by Sol Immobilization. *Langmuir* **2010**, *26*, 16568–16577.

(32) Choudhary, V. R.; Gaikwad, A. G.; Sansare, S. D. Activation of Supported Pd Metal Catalysts for Selective Oxidation of Hydrogen to Hydrogen Peroxide. *Catal. Letters* **2002**, *83*, 235–239.

(33) Samanta, C. Direct Synthesis of Hydrogen Peroxide from Hydrogen and Oxygen: An Overview of Recent Developments in the Process. *Appl. Catal. A Gen.* **2008**, *350*, 133–149.

(34) Samanta, C.; Choudhary, V. R. Direct Oxidation of H_2 to H_2O_2 over Pd/CeO_2 Catalyst under

Ambient Conditions: Influence of Halide Ions. *Chem. Eng. J.* **2008**, *136*, 126–132.

(35) Han, Y.-F.; Lunsford, J. H. Direct Formation of H_2O_2 from H_2 and O_2 over a Pd/SiO_2 Catalyst: The Roles of the Acid and the Liquid Phase. *J. Catal.* **2005**, *230*, 313–316.

(36) Landon, P.; Collier, P. J.; Carley, A. F.; Chadwick, D.; Papworth, A. J.; Burrows, A.; Kiely, C. J.; Hutchings, G. J. Direct Synthesis of Hydrogen Peroxide from H_2 and O_2 Using Pd and Au Catalysts. *Phys. Chem. Chem. Phys.* **2003**, *5*, 1917–1923.

Graphical Abstract: